# EFFECTS OF STREAMWISE ASPECT RATIO ON SPATIO-TEMPORAL CHARACTERISTICS OF RECTANGULAR CYLINDERS IN UNIFORM FLOWS

**Sedem Kumahor**
Department of Mechanical Engineering
University of Manitoba
Winnipeg, Manitoba, R3T 5V6, Canada
kumahors@myumanitoba.ca

**Mark F. Tachie**
Department of Mechanical Engineering
University of Manitoba
Winnipeg, Manitoba, R3T 5V6, Canada
mark.tachie@umanitoba.ca

## ABSTRACT

Turbulent flows over rectangular prisms with streamwise aspect ratios of AR = 1, 2 and 4 were experimentally studied using time-resolved particle image velocimetry at a Reynolds number (based on free-stream velocity and prism height) of 16200. These aspect ratios represent prisms for which the mean separated shear layers from the leading edges are shed directly into the wake region (AR1), reattach over the prism (AR4), and an intermediate case (AR2). The effects of aspect ratio on the mean flow are investigated using the streamwise mean velocity and wake recirculation length. The unsteady characteristics of the small-scale Kelvin-Helmholtz vortices and the energetic large-scale von-Kármán vortices are examined using frequency spectra of the streamwise velocity fluctuations, reverse flow area and proper orthogonal decomposition (POD). The ratio between the frequency associated with the Kelvin-Helmholtz vortices to the fundamental von-Kármán shedding frequency is shown to vary significantly with aspect ratio. The mean flow topology reveals a massive recirculation bubble in the wake of the AR2 prism, compared to AR1 and AR4. The differences in the vortex formation and shedding process are revealed in the dynamics of the first POD mode pair. A dual vortex shedding instability is manifested over the AR2 prism, which is shown to be intimately connected with the flow dynamics at the trailing edge. For AR1 and AR4, the first POD mode pair contain similar energy content, representing the large-scale von-Kármán vortices.

## INTRODUCTION

Separated shear layers induced by sharp-edged bluff bodies in uniform flows have been the subjected of extensive research over the past decades due to their prevalence in many industrial applications. At high Reynolds numbers (Re > 150), the flow separates at the sharp leading edge and either reattaches onto the prism if the streamwise aspect ratio (AR = $L/h$, where $L$ is streamwise length and $h$ is the prism height) is larger than 3.5 or shed directly into the wake region for the low aspect ratio prisms (AR < 2.0). The separated shear layer at the leading edge is characterized by small-scale Kelvin-Helmholtz (KH) vortices with characteristic high frequency that manifest as broadband peaks. The footprint of the energetic large-scale von-Kármán (VK) vortices that are shed alternately into the wake region manifests as dominant peaks at low-frequency. The interaction between the Kelvin-Helmholtz and von-Kármán vortices for a square prism has been examined in considerable detail (Brun et al., 2008; Trias et al., 2015; Lander et al., 2018; Moore et al., 2019), and the following correlation for the dependency of their frequency ratio on Reynolds number was proposed by Lander et al. (2018): $f_{KH}/f_{VK} = 0.18Re^{0.60}$. A rectangular prism with an aspect ratio of 5 was also investigated by Moore et al. (2019) and their results showed that $f_{KH}/f_{VK}$ is significantly lower than corresponding values for a square prism at similar Reynolds numbers. This observation demonstrates that the degree of interaction between the Kelvin-Helmholtz and von-Kármán vortices is dependent on their proximity or aspect ratio of the prisms.

The alternate shedding of the von-Kármán vortices results in the formation of coherent and chaotic fluctuating motions that interact non-linearly. Many techniques, including phase averaging (Hussain and Reynolds, 1970), linear stochastic estimations (Adrian, 1977) and proper orthogonal decomposition (Lumley, 1967) have been developed to extract and investigate the dynamics of the coherent structures. In recent years, proper orthogonal decomposition (POD) has gained popularity in extracting coherent structures from whole-field velocity data obtained using techniques such as particle image velocimetry (PIV). POD provides the optimal approximation of the flow field into a given number of modes. The first mode contains the highest turbulent kinetic energy content and in increasing mode number, a decrease in energy content. For flow over an Ahmed body, Thacker et al. (2013) showed that the first POD mode is associated with the low frequency flapping of the recirculation region over the rear slanted region. A similar observation was reported by Fang and Tachie (2019) and Kumahor et al. (2021) for flows over a forward-facing step. For flows over circular cylinders in uniform flow, Perrin et al. (2007) and Riches et al. (2018) have shown that the first POD mode pair is associated with the fundamental vortex shedding frequency. Similarly, van Oudheusden et al. (2005) and Mohebi et al. (2018) investigated coherent structures around rectangular prisms in uniform flow and showed that the first POD mode pair reveals the dominant flow features of the vortex shedding process. The above-mentioned studies have shown that the dynamics of the coherent structures can be described using POD. However, the interesting variations in the von-Kármán vortex shedding process around rectangular prisms in uniform flow over a wide range of streamwise aspect ratios is still not well understood.

Thus, the goal of the present study is to investigate the turbulent statistics as well as the spatial and temporal features of flows over a square prism (AR1) and rectangular prisms of

streamwise aspect ratio 2 (AR2) and 4 (AR4) using a time-resolved particle image velocimetry. Furthermore, POD analysis is performed to extract the dynamics of the coherent structures around the prisms. These aspect ratios are selected to ensure a direct shedding into the wake region (AR1), a mean reattachment onto the prism (AR4) and an intermediate case (AR2) where the separated shear layer does not reattach but exhibits a more complex dynamics compared to the square prism. In each case, velocity measurements were performed over the prism and near-wake region simultaneously to evaluate the interaction between the shear layer from the leading edge and the von-Kármán vortices.

## EXPERIMENTAL SET-UP

The experiments were performed in an open recirculating water channel at the University of Manitoba. The streamwise length, spanwise width and vertical height of the test section are 6000 mm, 600 mm and 450 mm, respectively. Three rectangular prisms with fixed vertical height, $h$ = 30 mm and spanwise width, $B$ = 580 mm were machined from smooth acrylic plates, with streamwise lengths of 30 mm (AR1), 60 mm (AR2) and 120 mm (AR4). The water depth was kept constant at 430 mm and the prisms were positioned such that the prism mid-height was 215 mm above the bottom wall. The free-stream velocity was set to $U_e$ = 0.540 m/s and Reynolds number based on cylinder height and free-stream velocity was 16200. The turbulence intensity ($Tu = \sqrt{\overline{u'u'}}/U_e$) measured at the channel mid-height in the absence of the cylinder was 1.2%.

Time-resolved particle image velocimetry was used to perform velocity measurements at the mid-span of the channel. The water was seeded with 10 µm silver coated hollow glass spheres with density of 1400 kg/m$^3$. A diode pumped dual-cavity high-speed Neodymium-doped yttrium lithium fluoride (Nd:YLF) laser with maximum pulse energy of 30 mJ/pulse for each cavity was used to illuminate the seeding particles. Two high speed 12-bit complementary metal oxide semiconductor cameras of resolution, 2560 pixel × 1600 pixel positioned side-by-side were used to simultaneously image the flow in two fields of view (FOV). Since the flow is symmetric about the prism centerline, the FOVs were chosen such that the region over the prism and the upper half of the wake region were captured. The dimensions of the FOVs over the prism and wake region were, respectively, 3.3$h$ × 2.1$h$ and 4.6$h$ × 2.9$h$, resulting in digital image resolutions of 25.0 pixel/mm and 18.4 pixel/mm, respectively. The sampling frequency was set to 800 Hz and 96000 images were captured for each test case. Data acquisition and image post-processing were performed using commercial software (DaVis version 10.0.5) supplied by LaVision Inc. Velocity vectors were calculated using a GPU-accelerated multi-pass cross-correlation algorithm with a single initial pass of 128 pixel × 128 pixel interrogation area (IA) with 50% overlap followed by four final passes of 24 pixel × 24 pixel IA with 75% overlap. The vector spacing was 0.20 mm (0.007$h$) and 0.33 mm (0.011$h$) for FOVs over the prisms and in the wake region, respectively. The resulting measurement uncertainty within 95% confidence level was 2.55% and 6.88% in the mean velocities and Reynolds stresses, respectively, at the locations of high local turbulence levels (Kumahor and Tachie, 2022).

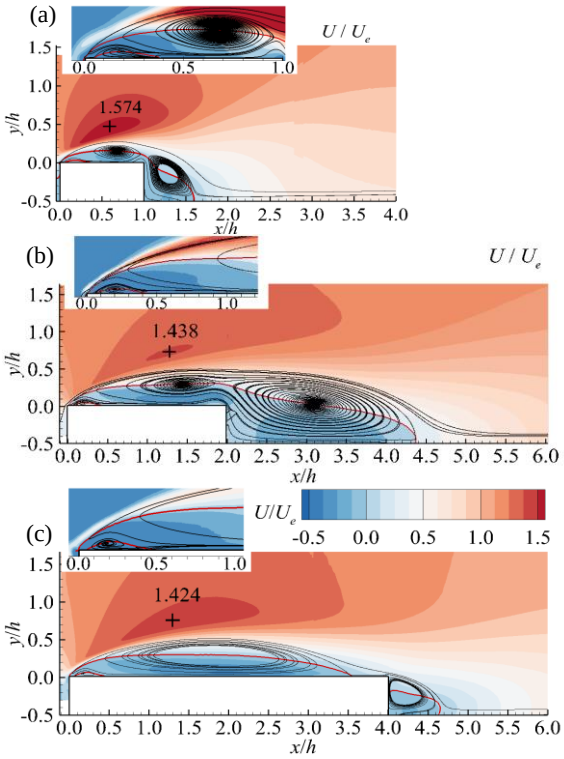


Figure 1: Mean streamwise velocity ($U$) for AR1 (a), AR2 (b) and AR4 (c), superimposed with the mean streamlines (black continous lines), isopleth of $U$ = 0 (red continuous lines) and symbol + marks the local peak over the cylinder with the respective magnitude written above. The insert in the top left corner shows contours of the turbulent kinetic energy near the leading edge.

## RESULTS AND DISCUSSION

Figure 1 shows contours of the mean streamwise velocity ($U$) superimposed with mean streamlines and the isopleth of $U$ = 0. The separated shear layer is directly shed into the wake region for AR1 and AR2, while mean reattachment occurs at $x/h$ = 3.6 over AR4. The recirculation lengths, which were determined as the streamwise distance between the trailing edge to location of $U$ = 0 along the symmetry plane, were $x/h$ = 0.60, 2.40 and 0.60, respectively, for AR1, AR2 and AR4. It was observed that instantaneous reattachment occurs over the cylinders 35%, 20% and 80% of the time for AR1, AR2 and AR4, respectively. Instantaneous flow visualization reveals that the backflow deflected upward at the trailing edge of AR2 significantly attenuates the reattachment of the separated shear layer. Consequently, the shear layer is streamwise elongated and descends further downstream into the wake region. Over the prisms, the maximum value of $U$ decreases monotonically with an increase in AR. Although not shown, the turbulent kinetic energy also decreases in magnitude as AR increases, with peak values of $0.5(\overline{u'u'} + \overline{v'v'})/\,U_e^2$ = 0.504, 0.202 and 0.072, respectively, for AR1, AR2 and AR4.

Figure 2 shows the premultiplied frequency spectra of streamwise fluctuating velocity at selected locations along the shear layers. Dominant peaks at Strouhal numbers corresponding to the fundamental von-Kármán shedding frequency for the three aspect ratios are evident in each plot, reflecting the global nature of the von-Kármán instabilities. The Strouhal number of $St_{VK}$ = 0.138, 0.084 and 0.134 for

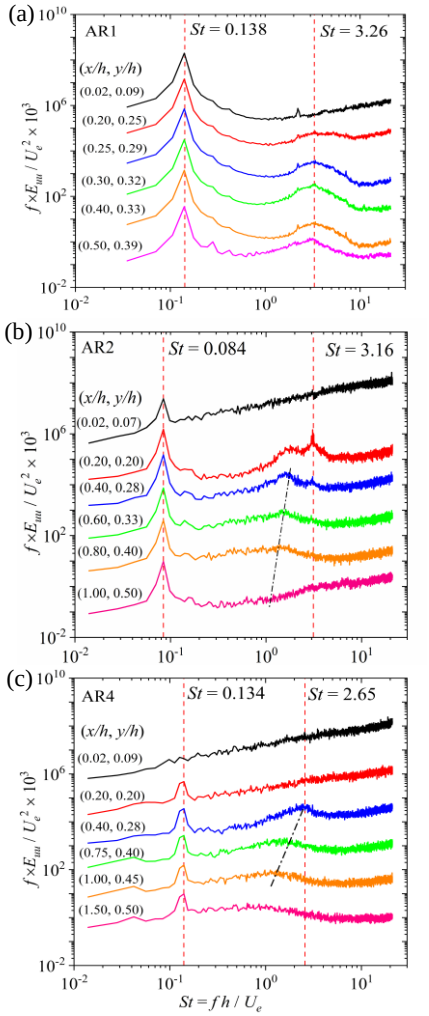


Figure 2: Premultiplied frequency spectra of the streamwise fluctuating velocity ($E_{uu}$) for AR1 (a), AR2 (b) and AR4 (c) at selected streamwise locations along the outer edge of the shear layer.

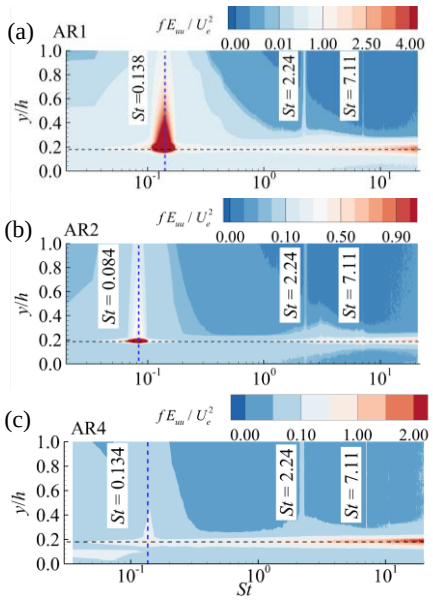


Figure 3: Contours of the premultiplied frequency spectra of the streamwise fluctuating velocity ($E_{uu}$) at $x/h$ = 0.20 AR1 (a), AR2 (b) and AR4 (c). Horizontal dashed lines represent the vertical location of the maximum turbulent kinetic energy.

AR1, AR2 and AR4, respectively, are in good agreement with prior studies (Okajima, 1982; Mohebi et al., 2017; Lander et al., 2018). Broadband high frequency peaks reminiscent of small-scale Kelvin-Helmholtz instabilities are also observed, however, these peaks are comparatively lower than the low frequency peaks and do not emerge until $x/h$ = 0.2 (for AR1 and AR2) and $x/h$ = 0.4 (for AR4). The frequencies associated with the Kelvin-Helmholtz instability for AR1 and AR2 are similar but relatively higher than for AR4. The values of $St_{KH}/St_{VK}$ = 24, 38 and 20 clearly demonstrate that the interaction between the small-scale and large-scale energetic vortices is not a linear function of aspect ratio. The spectral migration to lower frequencies observed in the spectra are due to the pairing of smaller vortices to form successively larger vortices with characteristic lower frequencies.

Contours of premultiplied frequency spectra of the streamwise fluctuating velocity at $x/h$ = 0.20 from the leading edge are shown in Figure 3. In addition to the peaks corresponding to the fundamental von-Kármán shedding frequencies and Kelvin-Helmholtz instabilities, distinct peaks are also observed at $St$ = 2.24 and 7.11, irrespective of aspect ratio. However, these higher frequency peaks do not exhibit the broadband characteristics of the Kelvin-Helmholtz instability. Previous studies over square cylinders reported broadband peaks at $St$ = 6 – 8 (Trias et al., 2015; Lander et al., 2018; Moore et al., 2019), and the limited information available in the literature suggests that the Kelvin-Helmholtz frequency varies with Reynolds number, turbulence intensity and blockage ratio (Brun et al., 2008).

Proper orthogonal decomposition (POD) is performed to extract the dominant coherent structures and examine their contributions to the vortex shedding process. In the current implementation of POD, the snapshot POD method proposed by Sirovich (1987) and detailed in Fang and Tachie (2019) is employed. The POD analysis is performed for all cases within the area $x/h \times y/h \in [0.0, 6.3] \times [-0.5, 1.5]$, subtracting the area determined as the prism. This implementation area was chosen to encompass the regions of elevated Reynolds stresses over and behind the prisms. As remarked by van Oudheusden et al. (2005) and Riches et al. (2018), two POD modes are typically required for a low-order representation of the coherent structures associated with the von-Kármán vortex formation and shedding process. The two modes, often referred to as the mode pair, must possess similar energy content. A cross plot of their temporal coefficients should form an ellipse and their spatial modes must be shifted by one-quarter wavelength ($\lambda$/4) of the coherent structures. With this framework, the POD mode information is examined to elucidate the influence of streamwise aspect ratio on the dynamics of the coherent structures.

Figure 4 shows the energy content of the first six most energetic POD modes. The total energy contribution of the first six modes is 75.2%, 68.6% and 63.3%, respectively, for AR1, AR2 and AR4. Meanwhile, the first mode pair contribute 66.3%, 54.2% and 54.7%, respectively, for AR1, AR2 and AR4. Consistent with the observations by van Oudheusden et al. (2005), Mohebi et al. (2018) and Riches et al. (2018), the first mode pair possess similar energy content for AR1 and AR4, indicating the dominance of the periodic von-Kármán vortices shed around both cylinders. On the other hand, the first POD mode is 43% higher than the second POD mode for AR2. The lower energy content in the second POD mode is attributed to the loss of coherence and the existence of a dual vortex shedding process, which was previously

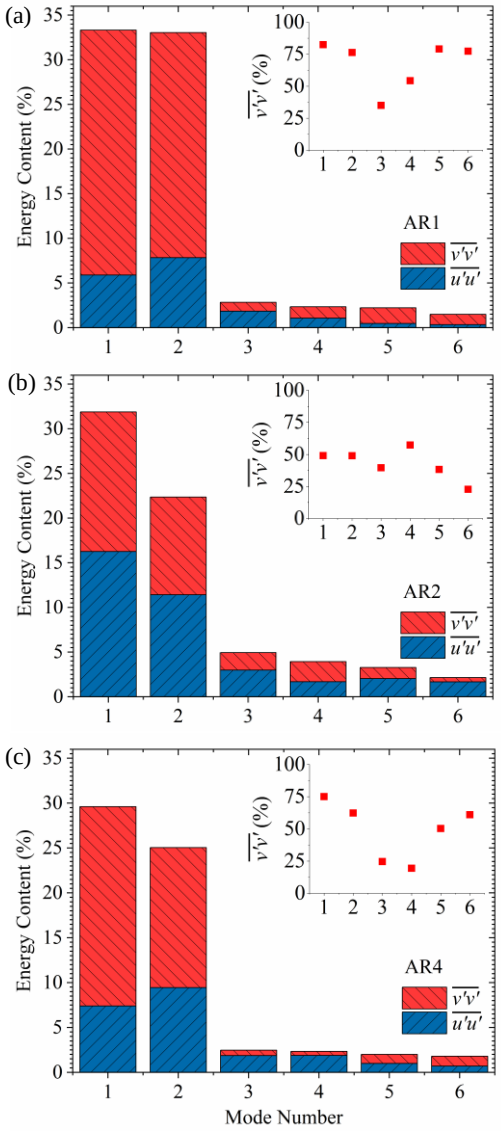


Figure 4: Relative contribution (%) to the TKE by the streamwise ($u'$) and vertical ($v'$) fluctuating components of the first six POD modes for AR1 (a), AR2 (b) and AR4 (d). Figure inserts present the percentage contribution of $v'$ to each mode.

reported in the literature (Okajima, 1982; Knisely, 1990; Mohebi et al., 2017). As shown in Figure 1(b) for AR2, the wake recirculation region is significantly larger due to the suppression of flow reattachment by the strong backflow emanating from the trailing edge. This suppression mechanism may lead to the formation of dual vortex shedding patterns over and behind the AR2 prism, which deviates from the conventional von-Kármán shedding process. Since the von-Kármán vortex shedding motions are dominated by vertical velocity fluctuations (Nakagawa et al., 1999; Kumahor and Tachie, 2022), the relative contributions of $v'$ to the energy content in each mode are presented by the red shaded regions of the bars and subsequently as inserts in Figure 4. The vertical fluctuations contribute to more than 65% of the energy content in the first mode pair for AR1 and AR4 but only 50% for AR2.

The cross plots of the temporal POD mode coefficients of the first mode pair are shown in Figure 5. The well-organized elliptical shape for AR1 and AR4 reveal that the coherent

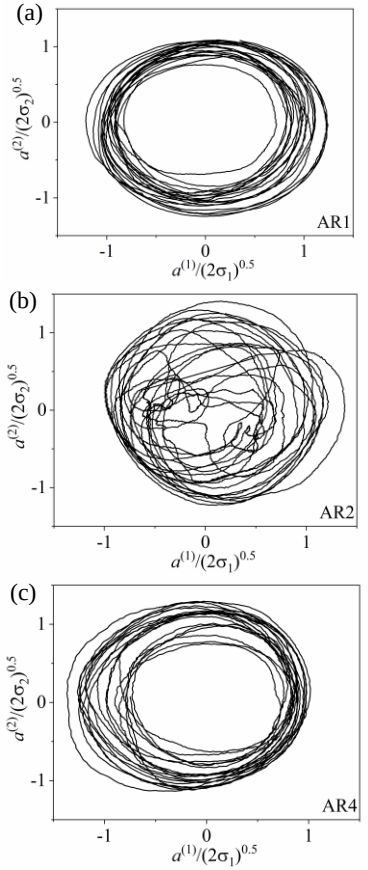


Figure 5: Cross plot of the temporal POD mode coefficients $a^{(1)}$ and $a^{(2)}$ for AR1 (a), AR2 (b) and AR4 (c).

structures are significantly more organized in AR1 and AR4, compared to AR2. This indicates significant cycle to cycle variation in the vortex shedding patterns over and behind the AR2 prism. Frequency spectra of the first four mode coefficients ($a^{(i)}$, where $i$ is the mode number) and radius calculated from the orbits in Figure 5 are presented in Figure 6. The results show dominant peaks at the fundamental shedding frequency for $a^{(1)}$ and $a^{(2)}$, irrespective of aspect ratio, suggesting that the first two modes are indeed associated with the von-Kármán vortices. These two modes also show subdominant peaks at the second harmonic for AR1 and AR4, and third harmonic in the case of AR4. The spectra of $a^{(3)}$ and $a^{(4)}$ reveal peaks at the fundamental shedding frequency and second harmonic for AR1, or the second and third harmonics for AR4. The peaks observed at these harmonics are a reflection of the breakup of large-scale vortices associated von-Kármán shedding vortices into smaller and smaller vortices.

The spectra of $a^{(1)}$ to $a^{(4)}$ for AR2 on the other hand, reveal a sub-dominant peak at a second frequency corresponding to $St$ = 0.145. The peaks occurring at $St$ = 0.084 and 0.145 is consistent with the dual vortex shedding frequencies reported by Okajima (1982) and Knisely (1990) for the AR2 prism. Reminiscing from Figure 2(b), it is evident that the peak at $St$ = 0.145 is not associated with the separated shear layer but only manifests within the wake region. This suggests that the state of the developing boundary layer near the trailing edge significantly impacts the dynamics of the vortex shedding process over the rectangular prisms. The radius calculated from the orbits of the first mode pair peak at

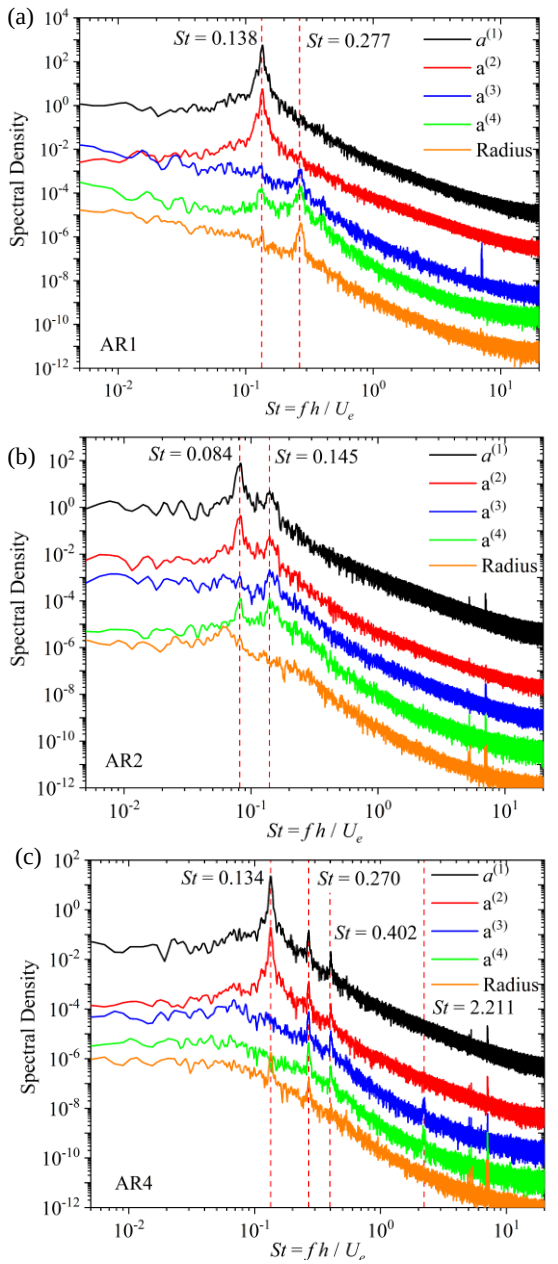


Figure 6: Frequency spectra of the first four POD mode coefficients and radius calculated from $a^{(1)}$ and $a^{(2)}$ for AR1 (a), AR2 (b) and AR4 (c).

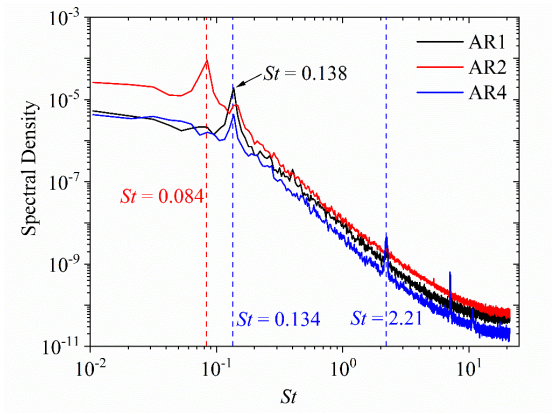


Figure 7: Frequency spectra of the reverse flow area

both the fundamental shedding frequency and its second harmonic for AR1 and AR4, meanwhile, no discernible peak is observed at either dual peaks for AR2.

Following Fang and Tachie (2019) and Kumahor et al. (2021), the temporal variation of the reverse flow area around the prisms are investigated, and the frequency spectra is presented in Figure 7. The results show that the enlarging and shrinking of the recirculation bubbles formed around the prisms occur at frequencies consistent with that observed in the first POD mode pair. Therefore, it is corroborated that the first POD mode pair is associated with the large-scale von-Kármán vortices shed over the rectangular prisms. It is worth noting that, the average reverse flow areas ($\bar{A}/h^2$) are 0.55, 1.53 and 1.13, respectively, for AR1, AR2 and AR4 indicating the massive size of the recirculation bubble around the AR2 prism (see Figure 1(b)).

Figure 8 shows the spatial contributions of the first POD mode pair by the vertical velocity fluctuations. Alternating positive and negative zones, representative of the von-Kármán shedding motions are evidenced in both modes. The vortex cores are observed near the symmetry plane within the wake region, signifying the symmetrical nature of the large-scale von-Kármán vortices. The distance between the negative and positive zo↓nes obtained from the first POD mode, which is representative of the half wavelength ($\lambda/2$) of the coherent structures, is typically used to calculate the convective velocity (Riches et al., 2018). The resulting convective velocity ( $U_c/U_e$ ) is 0.83 and 0.48 for AR1 and AR4, respectively. In the case of AR2, dual convective velocities $U_c/U_e$ = 0.35 and 0.61 that correspond to $St$ = 0.084 and 0.145, respectively, are obtained.

## CONCLUSION

The effects of streamwise aspect ratio (AR) on the turbulent flow around rectangular cylinders in uniform flow were experimentally investigated using a time-resolved particle image velocimetry system. The streamwise aspect ratios (streamwise length to height ratio) tested were AR =1, 2 and 4, corresponding to cases when the mean separated shear layers from the leading edges are shed directly into the wake region (AR1), reattach over the prism (AR4), and an intermediate case (AR2). The Reynolds number based on free-stream velocity and prism height was 16200.

The ratio between the frequency associated with the small-scale Kelvin-Helmholtz vortices occurring near the leading edge and the energetic large-scale von-Kármán vortices varies significantly with aspect ratio. This suggests that the interaction between the small-scale vortices that are formed in the shear layer at the leading edge and the large-scale vortices shed into the wake region is strongly dependent on their proximity. The mean flow features a massive recirculation region in the wake of the AR2 prism, compared to AR1 and AR4. Using proper orthogonal decomposition and the reverse flow area, the results for the AR2 prism show the existence of a dual vortex shedding process which is intimately tied to the flow dynamics occurring near the trailing edge. The strong back flow near the trailing edge for AR2 significantly attenuates the reattachment of the separated shear layer. For AR1 and AR4, the fundamental vortex shedding frequency is the dominant peak and the first POD mode pair contain similar energy percentages. This suggests regular von-Kármán shedding patterns over the AR1 and AR4 prisms.

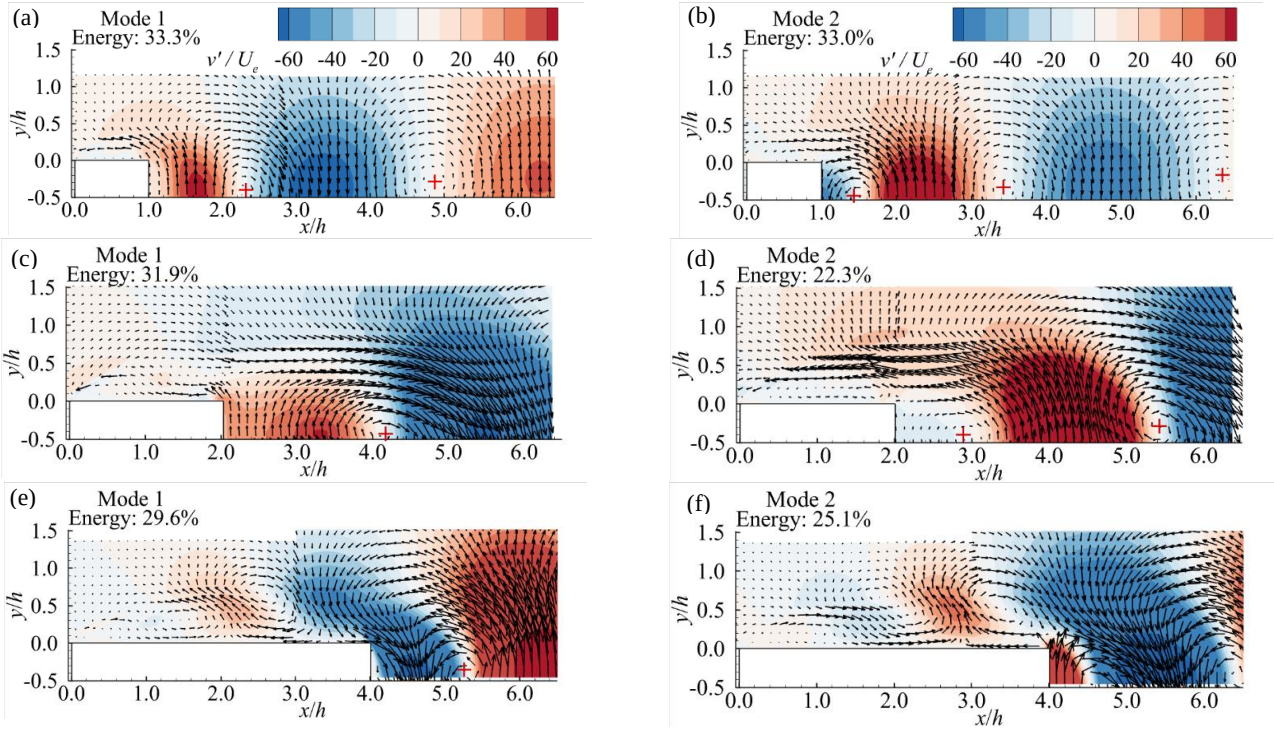


Figure 8: Contours of the first two POD modes using the vertical velocity fluctuations ($v'$) for AR1 (a,b), AR2 (c,d) and AR4 (e,f). The symbol (+) represents the vortex centers

## ACKNOWLEDGMENT

The funding support from the Natural Sciences and Engineering Research Council of Canada to MFT is gratefully acknowledged. We are also grateful to Canada Foundation for Innovation for funding for the experimental facility.

## REFERENCES

Adrian, R., 1977, "On the Role of Conditional Averages in Turbulence Theory". *In: Proc. Fourth Biennial Symp.on Turbulence in Liquids* New Jersey Science Press pp. 323-332.

Brun, C., Aubrun, S., Goossens, T., and Ravier, Ph., 2008, "Coherent structures and their frequency signature in the separated shear layer on the sides of a square cylinder", *Flow Turbulence Combust*, Vol. 81. pp. 97-114.

Fang X. and Tachie, M. F., 2019, "On the unsteady characteristics of turbulent separations over a forward-backward-facing step." *Journal of Fluid Mechanics*, Vol. 863, pp. 994-1030.

Franke, R., Rodi, W., and SchÖnung, B., 1990, "Numerical calculation of laminar vortex-shedding flow past cylinders", *Journal of Wind Engineering and Industrial Aerodynamics*, Vol 35, pp. 237-257

Knisely, C. W., 1990, "Strouhal numbers of rectangular cylinders at incidence: a review and new data", *Journal of Fluids and Structures*, Vol. 4, pp. 371-393.

Kumahor, S., Fang, X., and Tachie M. F., 2021, "The effects of upstream wall roughness on the spatio-temporal characteristics of flow separations induced by a forward-facing step", *Journal of Fluids Engineering*, Vol 143, pp. 071301.

Kumahor, S., and Tachie M. F., 2022, "Turbulent flow around rectangular cylinders with different streamwise aspect ratios". *Journal of Fluids Engineering*, Vol. 144, pp. 051304.

Lander, D. C., Moore, D. M., Letchford, C. W., and Amitay, M., 2018, "Scaling of square-prism shear layers", *Journal of Fluid Mechanics*, Vol. 849, pp. 1096-1119.

Lumley, J. L., 1967, "The structure of inhomogeneous turbulent flows". *In: Yaglom, A. and Tartarsky, V., Atmospheric Turbulence and Radio Wave Propagation*, pp. 166-177.

Mohebi, M., Plessix, P., Martinuzzi, R. J., and Wood, D. H., 2017, "Effect of thickness-to-chord ratio on the wake of two-dimensional rectangular cylinders". *Physical Review Fluids*, Vol 2, pp. 064702.

Moore, D. M., Letchford, C. W., and Amitay, M., 2019, "Energetic scales in a bluff body shear layer", *Journal of Fluid Mechanics*, Vol 875, pp. 543-575.

Nakagawa, S., Nitta, K., and Senda, M., 1999, "An experimental study on unsteady turbulent near wake of a rectangular cylinder in a channel flow", *Experiments in Fluids*, Vol. 27, pp. 284-294.

Okajima, A., 1982, "Strouhal numbers of rectangular cylinders", *Journal of Fluid Mechanics*, Vol 123, pp. 379-398.

Perrin, R., Braza, M., Cid, E., Cazin, S., Barthet, A., Sevrain, A., Mockett, C. and Thiele, F., 2007, "Obtaining phase averaged turbulence properties in the near wake of a circular cylinder at high Reynolds number using POD". *Experiments in Fluids*, Vol 43, pp. 341-355.

Riches, G., Martinuzzi R., and Morton, C., 2018, "Proper orthogonal decomposition analysis of a circular cylinder undergoing vortex-induced vibrations". *Physics of Fluids*, Vol 30, pp. 105103.

Sirovich, L., 1987, "Turbulence and the dynamics of coherent structures. Part I, II and III". *Quarterly of Applied Mathematics*, Vol. 45, pp. 561-571.

Trias, F., Gorobets, A., and Olivia, A., 2015, "Turbulent flow around a square cylinder at Reynolds number 22,000: A DNS study", *Computers and Fluids*, Vol. 123, pp. 87-98.

van Oudheusden B. W., Scarano, F., Hinsberg, N. P. and Watt, D. W., 2005, "Phase-resolved characterization of vortex shedding in the near wake of a square-section cylinder at incidence". *Experiments in Fluids*, Vol 39, pp. 86-98.